

*Biogeochemistry* **59:** 69–94, 2002.


# Atmospheric emission and cycling of carbon monoxide in the Scheldt Estuary

C.S. LAW*, T.N. SJOBERG & R.D. LING
*Plymouth Marine Laboratory, Prospect Place, The Hoe, Plymouth, Devon, PL1 3DH U.K.*
*(*Author for correspondence; present address: National Institute of Water and Atmospheric Research (NIWA), Wellington, New Zealand; e-mail: c.law@niwa.cri.nz)*

Received 4 May 2000

**Key words:** carbon monoxide, dissolved organic carbon, emission, estuaries, microbial oxidation, photo-production

**Abstract.** Axial profiles of dissolved carbon monoxide (CO) from four surveys of the Scheldt estuary confirmed that the estuary is a source of atmospheric CO, with an emission range of 4–404 nmol $m^{-2}$ $h^{-1}$. Surface water CO concentration and atmospheric emission were spatially variable, with an order of magnitude difference between the upper and lower estuary in spring, and seasonally variable with highest levels in spring and lowest in winter. Annual CO emission was estimated to be 700 (396–1032) $\times$ $10^3$ mol, equivalent to 0.02–0.05% of dissolved organic carbon (DOC) input to the estuary. CO photoproduction rates were an order of magnitude greater in the upper estuary in spring and correlated with DOC concentration. Total CO production from DOC photodegradation was estimated to be 8.5–18 $\times$ $10^3$ mol CO $d^{-1}$, equivalent to 0.21–0.44% of riverine DOC input in spring. The deficit between production and emission suggests that microbial CO oxidation accounts for 68% of photoproduced CO, with highest oxidation rates at low salinities. The results indicate that suspended particulate material indirectly influences estuarine CO distribution and emission. Assuming that the Scheldt is representative, estuaries do not contribute significantly to the oceanic or global CO budgets.

## Introduction

The trace gas carbon monoxide (CO) plays a critical role in the maintenance of the atmospheric chemical composition by influencing the hydroxyl radical concentration and so the tropospheric oxidative capacity. As a result it influences the residence time of methane and halocarbons, and indirectly the greenhouse effect and stratospheric ozone depletion (Sze 1977). The CO molecule is also infrared-active and contributes to the greenhouse effect directly (Evans & Puckrin 1995). In addition, the photooxidation of CO in the presence of $NO_x$ contributes to the tropospheric production of ozone resulting in a summer maximum in northern mid-latitudes (Watson et al.

1990). The residence time of CO is relatively short, on the order of 2–10 months (Bekki et al. 1994), and consequently atmospheric levels respond rapidly to alterations in source/sink strength. The atmospheric burden of CO primarily derives from anthropogenic sources such as fossil fuel combustion and biomass burning, and photochemical oxidation of methane and non-methane hydrocarbons (Cicerone 1988). A recent decline in atmospheric CO has been attributed to stratospheric ozone depletion (Bekki et al. 1994), and a decrease in anthropogenic output, suggesting that natural sources of CO may become more significant to the total atmospheric burden.

The oceanic CO flux of 100–165 Tg $yr^{-1}$ accounts for 3–10% of the total global flux (Cicerone 1988; Erickson 1989), although a recent re-assessment of oceanic emissions suggests it may be as low as 12.9 Tg $yr^{-1}$ (Bates et al. 1995). The origin of CO in surface waters is the photo-oxidation of dissolved organic carbon predominately by Ultra-Violet radiation (280–390 nm) (Naijar et al. 1995; Valentine & Zepp 1993), which results in a sinusoidal CO diel profile in the ocean with maximum concentrations in early-mid afternoon. Surface dissolved CO exhibits a concentration gradient from oligotrophic to productive oceanic regions, and positive relationships with dissolved organic carbon (DOC), productivity, nutrients and fluorescence have been identified (Setser 1982; Johnson & Bates 1996). These parameters all exhibit elevated levels in estuarine and coastal waters, suggesting that these regions may support a significant CO source.

Estuaries represent the primary conduit for the transfer of terrestrial organic carbon to the oceans, with an estimated global export of 0.2 Gt $y^{-1}$. DOC is subject to a variety of removal processes, including flocculation, respiration and adsorption/desorption as it is transferred from river to sea. Yet these transformations do not significantly influence the axial profile, and DOC generally behaves conservatively in estuaries (Mantoura & Woodward 1983; Alvarez-Salgado & Miller 1999). Conversely, other studies indicate that DOC in the ocean is predominately marine in origin, with less than 10% of terrestrial origin (Williams & Druffel 1987; Hedges et al. 1992), suggesting that an important sink process has been overlooked. Terrestrial DOC is biologically refractory but has a high photoreactivity and efficiency in the absorption of sunlight (Valentine & Zepp 1993). Potential CO production from wetlands alone may account for 300–400 Tg C $yr^{-1}$ (Valentine & Zepp 1993), which when compared with the total marine flux of 12.9 Tg $yr^{-1}$ (Bates et al. 1995) suggests considerable potential for DOC photodegradation to CO in estuaries and coastal waters. Estuaries are significant sources of atmospheric gases, such as carbon dioxide (Frankignoulle et al. 1998), methane (Scranton & McShane 1991) and nitrous oxide (Law et al. 1992; De Wilde & De Bie 2000). Yet photodegradation of DOC in estuaries

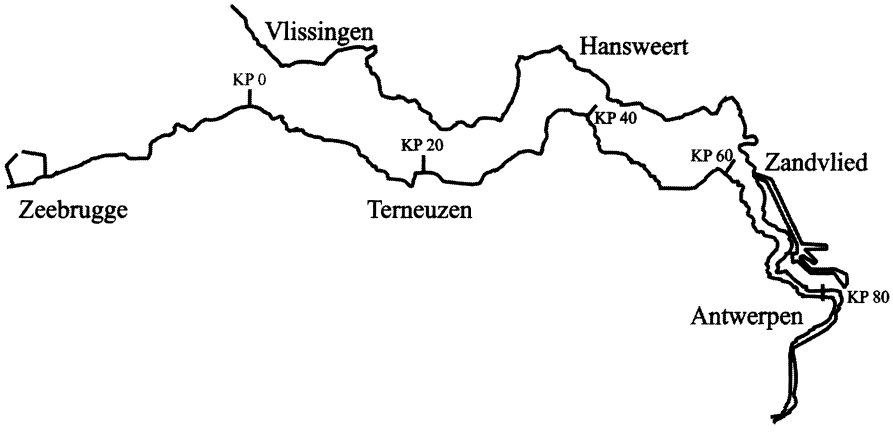


*Figure 1.* Map of the Scheldt Estuary, showing distance from the estuary mouth in kilometres and the main population centres.

and the associated production of volatiles such as CO and carbonyl sulphide have received little attention. The following study represents a component of the BIOGEST (Biogenic Gas Transfer in Estuaries) programme, and describes the first reported seasonal study of CO concentrations, emissions, and photochemical production rates in an estuary.

## Sampling and methodology

### *Survey site*

The Scheldt estuary derives from a catchment area of $22 \times 10^3$ km$^2$, which includes regions within France, Belgium and the Netherlands, and discharges into the southern North Sea (see Figure 1). The total river length is 355 km with a mean flow volume on the order of 100 m$^3$ s$^{-1}$, and seasonal variation between 60 m$^3$ s$^{-1}$ in summer to 180 m$^3$ s$^{-1}$ in winter (Baeyans et al. 1998). Freshwater outflow is small relative to tidal exchange, and so the estuary is tidally-dominated with a water residence time in the upper estuary of 2–3 months. The river basin supports 7 million inhabitants and significant industrial activity, and the estuary receives an organic carbon loading of $260 \times 10^9$ g C y$^{-1}$ (Wollast 1988). This predominately accumulates in the upper estuary where heterotrophic bacterial production rates are amongst the highest recorded (Goosen et al. 1995), resulting in water column oxygen depletion coincident with a turbidity maximum in the 2.5–5 salinity range.

*Dissolved CO*

[CO] was measured in surface waters of the Scheldt estuary during July and December 1996 (Scheldt 1 and 2, respectively) and May and October 1998 (Scheldt 3 and 4, respectively) aboard the *R/V Belgica*. The estuarine profile was characterised over a five-day period with sampling stations at salinity intervals of ~2.5 on the psu scale. Dissolved carbon monoxide ([CO]) was analysed in both discrete water samples and in underway mode using a perspex showerhead-type equilibrator. Surface water was pumped to the equilibrator from an intake in the bow of the *R/V Belgica* at 2.5 m depth. The equilibrator headspace was sampled 30 minutes after arrival on station to ensure headspace equilibration with local surface water. Discrete water samples were also collected on station from the 2.5 m intake and from Niskin bottle samples collected at 1 m depth. High-resolution vertical profiles of the upper 1 m were also obtained using a surface profiler deployed at distance from the *R/V Belgica*. This consisted of a free-floating buoy supporting four peristaltic pumps which sampled water from fixed depths of 10 cm, 25 cm, 50 cm and 1 m (May) or 2 m (October) below the surface. Sample bottles were flushed for five minutes to ensure expulsion of residual water and air in the lines.

All discrete water samples were collected in 125 ml glass serum bottles and sealed by gas-tight Teflon-lined butyl rubber seals. To create a headspace 17 (+/– 0.47) ml of CO-free zero-grade air was injected under minor positive pressure into each bottle, with expulsion of an equivalent volume of water sample. Tests on the serum bottles, equilibrator and high-resolution vertical profiler in the laboratory and field confirmed that there was no production of CO during sample collection and analysis. The headspace and sample were equilibrated for a period of 20 minutes using a wrist action shaker, after which the headspace gas was injected into a 1 ml stainless steel sample loop maintained at 40 °C. The same approach was used for equilibrator headspace and atmospheric samples, with air collected by syringe whilst the vessel was in motion. After a 20-second delay for sample loop pressure equalisation, the loop contents were injected into a zero-grade air carrier (flow 25 ml/min) which had been pre-purified with Hopcalite, and onto a 1 m 13X Molecular Sieve 60/80 mesh column for chromatographic separation. Detection of CO was by a Reduction Gas Detector (RGD2, *Trace Analytical*) in which mercuric oxide is reduced to mercury vapour as CO is oxidised to $CO_2$. The mercury vapour is produced stoichiometrically to CO and detected by absorption of UV radiation with a precision of 1 ppbv CO and linearity to >1 ppmv. Data capture was by PC interfaced integrator. CO calibration standards (364–462 ppbv) were cross-calibrated with a reference calibration gas (NOAA CMDL, 167 +/– 1.3 ppbv) before each survey. [CO] was calcu-

lated using the solubility coefficients of Weisenburg and Guinasso (1979) at equilibration temperature and salinity. CO saturation was expressed as the percentage difference between [CO] and the expected concentration $CO_E$, which was derived from the atmospheric CO concentration and the solubility coefficient at *in situ* temperature and salinity.

*Ancillary measurements*

A spectrophotometer on an adjustable mounting supported between three buoys was deployed at distance from the *R/V Belgica* to determine UV light penetration in surface waters during October. Sub-surface light spectra were obtained at the surface, 24 cm and 48 cm by a submersible fibre optic spectrophotometer (Ocean Optics S2000), with a nominal aperture size of 50 $\mu$m, wavelength range of 200–850 nm and resolution of 0.3 nm. Attenuation coefficients were calculated from:

$$Kd = \ln(E_s/E_z)/dz$$

where $E_S$ and $E_z$ represent irradiance at the surface and 24 cm, respectively and z is depth. Axial profiles of suspended particulate material (SPM) and DOC were also obtained. DOC samples were filtered using an all glass filtration unit through precombusted Whatman GF/F filters into precombusted glass ampoules, and acidified with 50% $H_3PO_4$ to a pH <2. DOC analysis was performed by a HTCO method (DIMA-TECH 100) and infrared detection of $CO_2$, with samples analysed in quadruplicate and a resultant precision of ± 3%. Surface water temperature and salinity were recorded using a Seabird Thermosalinograph SBE21, and windspeed and direction by a meteorological package located on the vessel at a height of 10 m. Instantaneous windspeeds averaged over a one-hour period during station occupancy were used to calculate air-water fluxes.

*Photoproduction experiments*

CO photoproduction rates were determined using water from the 2.5 m supply which was transferred into 300 ml silica bottles (Uher & Andreae 1997). Samples were irradiated under natural light in a deck incubator at surface water temperature for 2.5–4.5 hours. Time zero samples were analysed using the discrete sample method, and irradiated samples analysed at intervals of 0.75–1.25 hours. Dark controls were sealed in 125 ml serum bottles, wrapped in aluminium foil to eliminate light and maintained at *in situ* surface water temperature. Broad band UV light intensity on deck was measured using a Delta-T UVAB/P sensor fitted with a pre-amplifier. The spectral response was

determined as 100% at 360 nm at a bandwidth of 72 nm. Sensor output in mV was logged as 60-second average integrated values, temperature-corrected and converted to W $m^{-2}$. Shading of the sensor and incubation chamber was minimal, and the incubated samples were immersed to half-depth to minimise excess exposure to UV light.

*Air-sea exchange*

Atmosphere-ocean fluxes are generally calculated using a transfer velocity ($K_{600}$) derived for $CO_2$ and corrected for CO, and the observed CO gradient at the air-water interface. In this study, a $K_{600}$ parameterisation was used which was derived from dual tracer experiments in the tidal Hudson River and mass balance estimates in San Francisco Bay, and so is representative of gas exchange under estuarine and coastal conditions (Clark et al. 1995). This was considered most appropriate for the calculation of Scheldt CO emissions, particularly as the water column depth of 4–14 m in the Hudson River experiments was similar to that of the majority of the Scheldt estuary. A feature of this parameterisation is a non-zero intercept, indicative of enhanced exchange at very low windspeeds and attributable to processes such as boundary turbulence and tidal action which are characteristic of estuaries. The transfer velocity, $K_{600}$ is expressed as:

$$K_{600} = 2.0 + 0.24\, U_{10}^2$$

where $U_{10}$ is windspeed measured at a height of 10 m (Clark et al. 1995). $K_{CO}$ was calculated from $K_{600}$ by correcting for the diffusivity of CO (Wise & Houghton 1968) and the kinematic viscosity at *in situ* temperatures and salinities. CO emissions were calculated from the observed [CO] and atmospheric CO which exhibited variability on short timescales and distance (see Table 1). Each station measurement was obtained under variable light conditions at different times of the day (between 0800 and 1900), with no apparent diel trend in [CO]. In the ocean where light is the primary determinant [CO] exhibits a diel trend with a mid-afternoon maximum. However, this cannot be assumed for estuaries as diel variability may be obscured by regional variation in dissolved CO input and atmospheric CO, and tidal variation in the distribution of SPM and microbial oxidation. Furthermore the strong attenuation of light and enhanced vertical and lateral mixing and transport in estuaries may reduce the magnitude of any diel trend. Although no diel trends in [CO] have been published for estuaries, our measurements at two upper and one lower estuary site in the Humber did not identify a systematic diel trend in [CO] (Sjoberg 1999). Consequently we have used the observed [CO] as a mean diel concentration for the emission estimates, rather than introduce further uncertainty by the assumption of systematic diel variation.

*Table 1.* Mean atmospheric CO for the four Scheldt estuary surveys, with the Northern hemisphere average included for comparison

| Estuary | Month | Mean CO (ppbv) | Standard deviation (ppbv) |
|---|---|---|---|
| Scheldt 1 | July 1996 | 149.1 | 70.0 |
| Scheldt 2 | December 1996 | 452.4 | 137.9 |
| Scheldt 3 | May 1998 | 231.5 | 56.1 |
| Scheldt 4 | October 1998 | 454.1 | 160.4 |
| Northern Hemisphere | Watson et al. 1990 | 120.0 | |

## Results

### *(a) Atmospheric CO*

Atmospheric CO showed significant variation along the estuary and between surveys with 24–46% variability within each 4–5 day survey (see Table 1). On greater temporal and spatial scales the variability arises from the relative short atmospheric lifetime of CO of 1–2 months, and the influence of wind vectors which determine local air mass. The Scheldt estuary may be exposed to relatively clean air masses originating offshore or continental air masses containing significant anthropogenic CO. The mean atmospheric CO for each survey exceeded the mean Northern hemisphere CO (Watson et al. 1990), indicating that the local air masses had experienced significant anthropogenic input. The variability is further compounded by natural seasonal variation, which is characterised by lower atmospheric CO in summer due to an enhanced reaction rate with hydroxyl radicals (Bekki et al. 1994). The CO oxidation sink is lower in winter coincident with an increase in the atmospheric CO burden from combustion and other anthropogenic sources. This is reflected in the Scheldt data where the mean spring/summer atmospheric CO was one-third to half that of the autumn/winter (Table 1).

Variation in atmospheric CO can also occur on considerably shorter timescales. For example, atmospheric CO increased by 600 ppbv within a three-hour interval at a U.K. coastal sampling station in response to the transport of a polluted air mass (Cardenas et al. 1998). Variability along the Scheldt estuary resulted from localised point sources such as refineries and industry, mobile sources such as shipping, and temporal point sources associated with increased combustion emissions during peak travel periods. The variability of atmospheric CO at any point in an estuary can only be determined by continuous monitoring, which was impractical within the

framework of this study. There were no consistent trends in atmospheric CO along the estuary, although the outer estuary values were generally lower in May and July. As the water residence time in the upper estuary is on the order of 1–2 months, surface water was assumed to be in equilibrium with the local atmospheric CO. Consequently, the mean atmospheric CO for each survey (Table 1) was used with the respective *in situ* water temperature, to calculate $CO_E$ for each sample. $CO_E$ was lowest at 0.14 nmol $l^{-1}$ in the outer estuary in July and maximal at 0.66 nmol $l^{-1}$ at the head of the estuary in December (Figure 2).

*(b) Dissolved CO*

Significant variability was apparent in [CO] at 2.5 m depth, both within each survey and between surveys. A general trend was apparent with higher concentrations in the more saline waters of the outer estuary in May and July (see Figure 2), with a maximum [CO] of 4.5 nmol $l^{-1}$ during May, declining to 1 nmol $l^{-1}$ in July and October. This contrasts with other observations in Yaquina Bay, Oregon where [CO] was highest at low salinities (Butler et al. 1987). A maximum [CO] of 1 nmol $l^{-1}$ was observed at 2.5 m at the head of the Scheldt in December, with concentrations declining sharply and remaining constant at ~0.3–0.4 nmol $l^{-1}$ to the estuary mouth. Samples collected at 1 m depth using Niskin bottles exhibited similar axial trends in [CO], although were generally higher than at 2.5 m (see Figure 2). High-resolution vertical profiles of [CO] were also collected in the surface 1 m and 2 m during May and July, respectively. Despite restricted penetration of light no gradient was apparent between 10 and 100 cm in the upper estuary (see Figure 3), whereas surface [CO] at 10 cm exceeded that at 1 m by a factor of 2 at higher salinities in May. Conversely, [CO] remained constant throughout the upper 2 m in October (see Figure 3). Despite the absence of a gradient, samples collected at all depths by the high-resolution vertical profiler and 1 m Niskin bottle had higher [CO] than the 2.5 m depth samples. This discrepancy did not arise from methodological differences as discrete [CO] samples from the 2.5 m intake showed good agreement with equilibrator results during July and October (see Figure 2). This suggests that there is a decline in [CO] between 2 and 2.5 m, which may have been accentuated by loss of dissolved CO in the ships surface pumped supply. Regardless of the source of this discrepancy, the [CO] at 2.5 m would provide an underestimate of CO emission, and so degrees of saturation and emissions were estimated from the 10 cm depth samples for May and October, and by extrapolation from the 10 cm:2.5 m ratio for July and December. Figure 4 illustrates strong seasonal and spatial variability in CO saturation, with saturation in the outer estuary exceeding that of the upper estuary by an order of magnitude in May. In

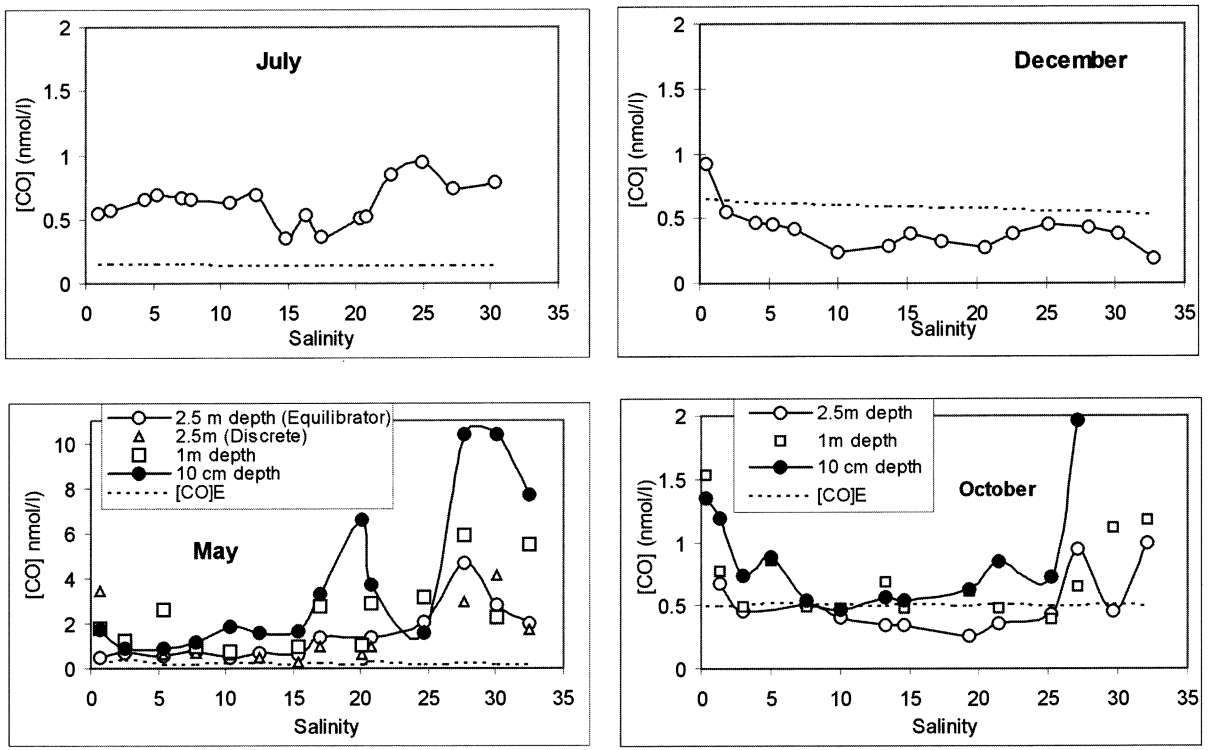


*Figure 2.* Axial profiles of [CO] (open circles) at 2.5m depth and $[CO]_E$ (dashed line) for the four Scheldt surveys (see key for additional depth measurements). Note change in y-axis scale for May.

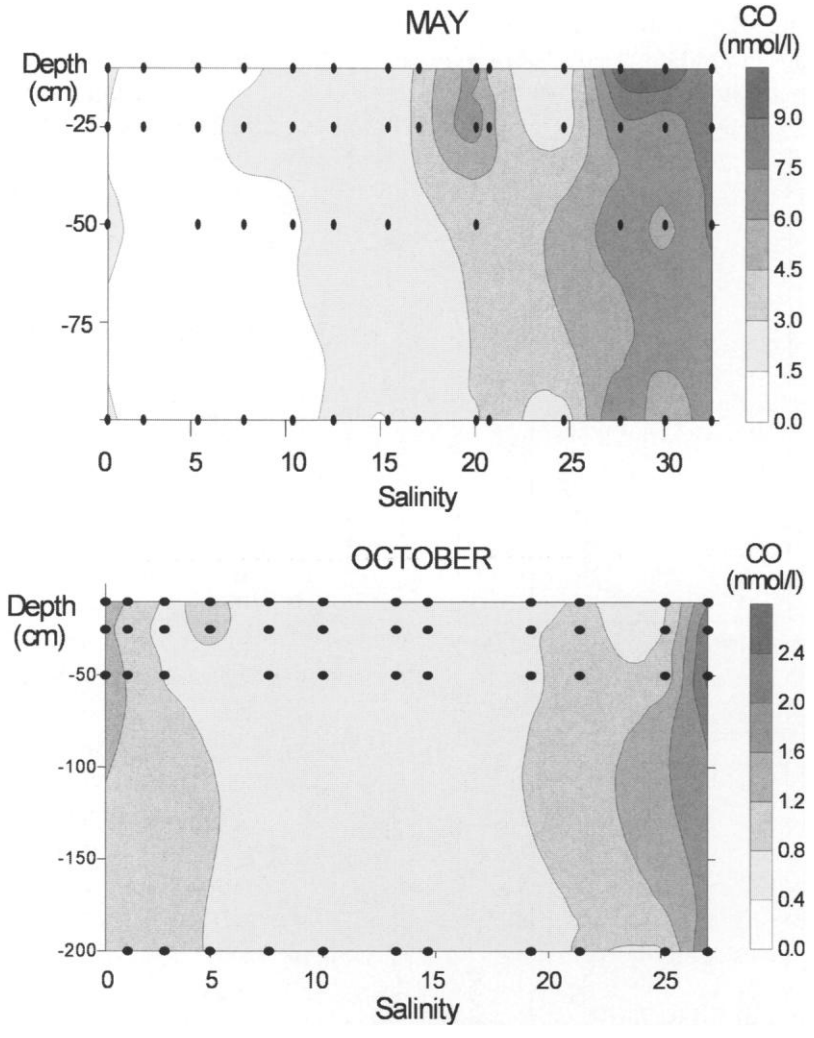


*Figure 3.* Axial transect of high resolution vertical [CO] profiles in surface waters during May (upper) and October (lower). Note that maximum sample depth was 1 m during May and 2 m during October.

contrast the estuary was close to equilibrium in winter, although the seasonal difference in saturation was enhanced by lower atmospheric CO in summer and higher in winter.

*(c) Ancillary variables*

SPM generally exhibited a primary maximum at the head of the estuary, with a smaller secondary maximum in the mid-estuary in spring and summer

(Figure 4). No seasonal trend was apparent in the magnitude of the SPM maximum, although SPM was generally lower in the outer estuary during May and July. Although a significant relationship was not apparent, elevated SPM coincided with lower [CO] in the upper estuary, and elevated [CO] with low SPM in the outer estuary during May and July. This was most apparent in the mid-estuarine region in July where a sharp SPM maximum coincided with a [CO] minimum (Figure 4).

The depth of the euphotic zone in the Scheldt estuary is between 8 and 0.8 m (Kromkamp et al. 1995), and undoubtedly limits photolytic processes. UV radiation is more rapidly attenuated than longer wavelengths, and penetration is dependent on the degree of absorption and scattering. Action spectra have shown that photochemical production of CO is highest in the UV-B waveband (280–320 nm) and declines exponentially with increasing wavelength, although production is still significant in the UV-A range (320–390) and the blue end of the visible spectrum (Valentine & Zepp 1993; from Naijar et al. 1995). Although UV-A has a lower photoproductive potential for CO (Naijar et al. 1995) it is attenuated at a lower rate than UV-B and consequently penetrates the water column to a greater depths. The penetration of photochemically effective irradiance was defined in this study by the 360 nm wavelength, which was considered representative for UV-A and UV-B. The sub-surface light field showed increased penetration across the spectrum in the outer estuary. UV penetration was limited in the turbid upper estuary to <25 cm and UV was undetectable at 48 cm throughout the estuary (Figure 5). The UV attenuation coefficient, Kd, was maximal in the turbid upper estuary (24.6 $m^{-1}$) and declined to 5.8 $m^{-1}$in the outer estuary (see Figure 6). DOC is a major determinant of UV attenuation and exhibited a similar distribution to Kd, declining from the upper estuary to the mouth as observed in other estuaries (Mantoura & Woodward 1983; Alvarez-Salgado & Miller 1999; Miller 1999). No significant relationship was observed between [CO] and DOC or Kd in May or October (see Figures 2, 6 and 8).

*(d) Photoproduction*

The photo-irradiation incubations were performed between 1000 and 1630 during which UV irradiance remained relatively constant (see Figure 7). Potential CO photoproduction was linear during the incubations, with production rates of 1–10.6 nmol $l^{-1}$ $h^{-1}$ $(W\ m^{-2})^{-1}$ and a mean standard error of 20% (see Figure 8). These rates are regarded as potential rather than actual due to the favourable conditions for exposure to light. Potential CO photoproduction rates co-varied with DOC with highest rates in the upper estuary decreasing to the mouth, and a factor of 10 difference between end-members (see Figure 8). The 2.5 salinity station exhibited an anomalously low potential

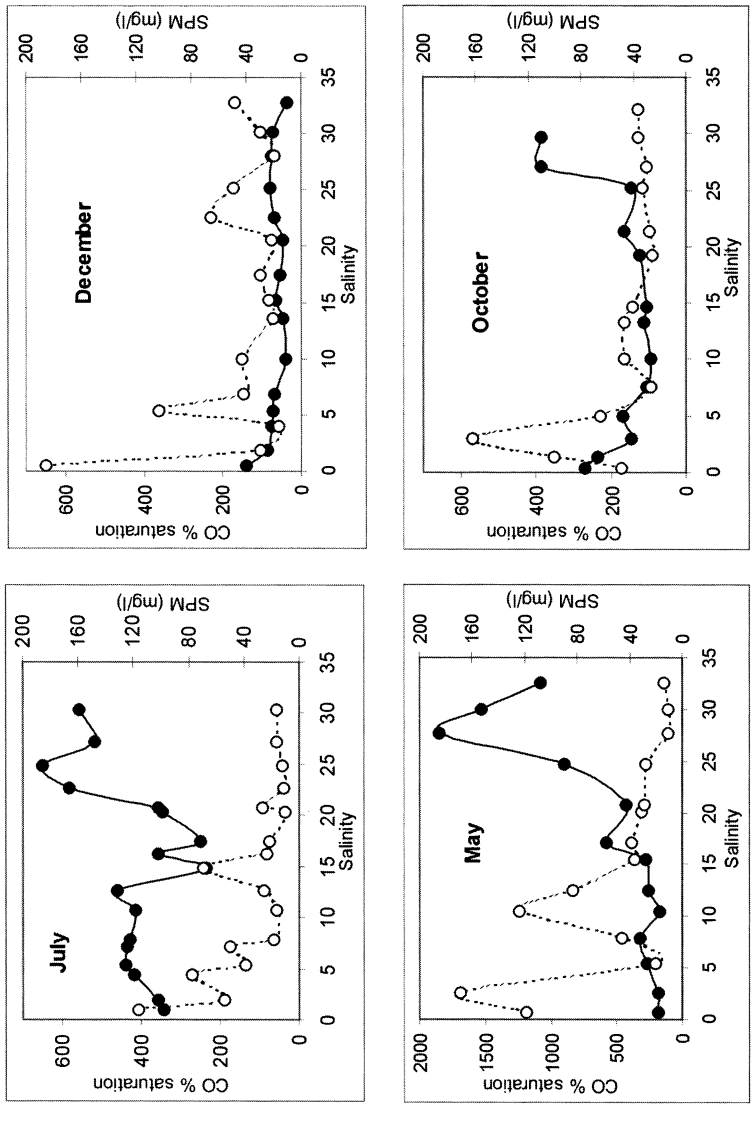


*Figure 4.* Axial profiles of CO% saturation (filled circles) and SPM (open circles) for the Scheldt estuary surveys. Note change in y-axis scale for May.

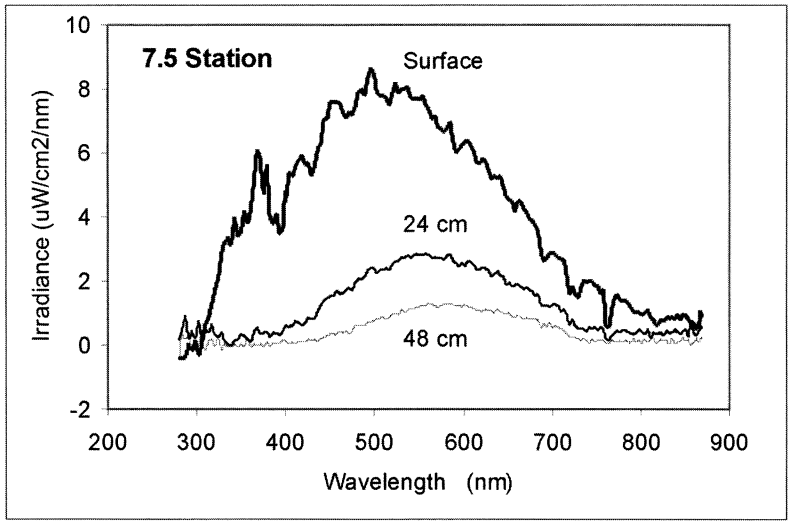


*Figure 5.* Light spectrum profile at the surface, 24 cm and 48 cm depth at the 7.5 salinity station in May.

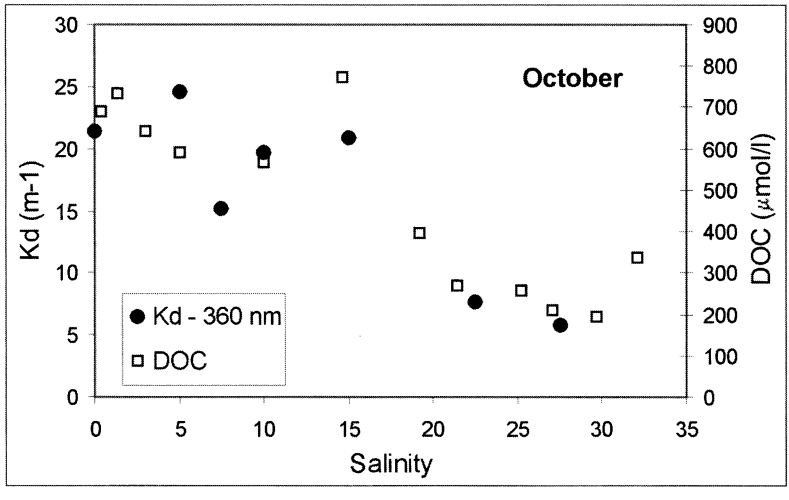


*Figure 6.* Axial profile of Kd at 360 nm (filled circles) and DOC (open squares) in October.

photoproduction rate and was excluded from further interpretation. The dark controls did not exhibit any significant loss of CO during the incubations (see Figure 7), in contrast to results obtained in the Humber and Tamar estuaries using this technique (Sjoberg 1999).

Daily potential CO photoproduction rates were estimated using the total daily photoeffective light (313.9 kJ $m^{-2}$) as determined from broad-band UV

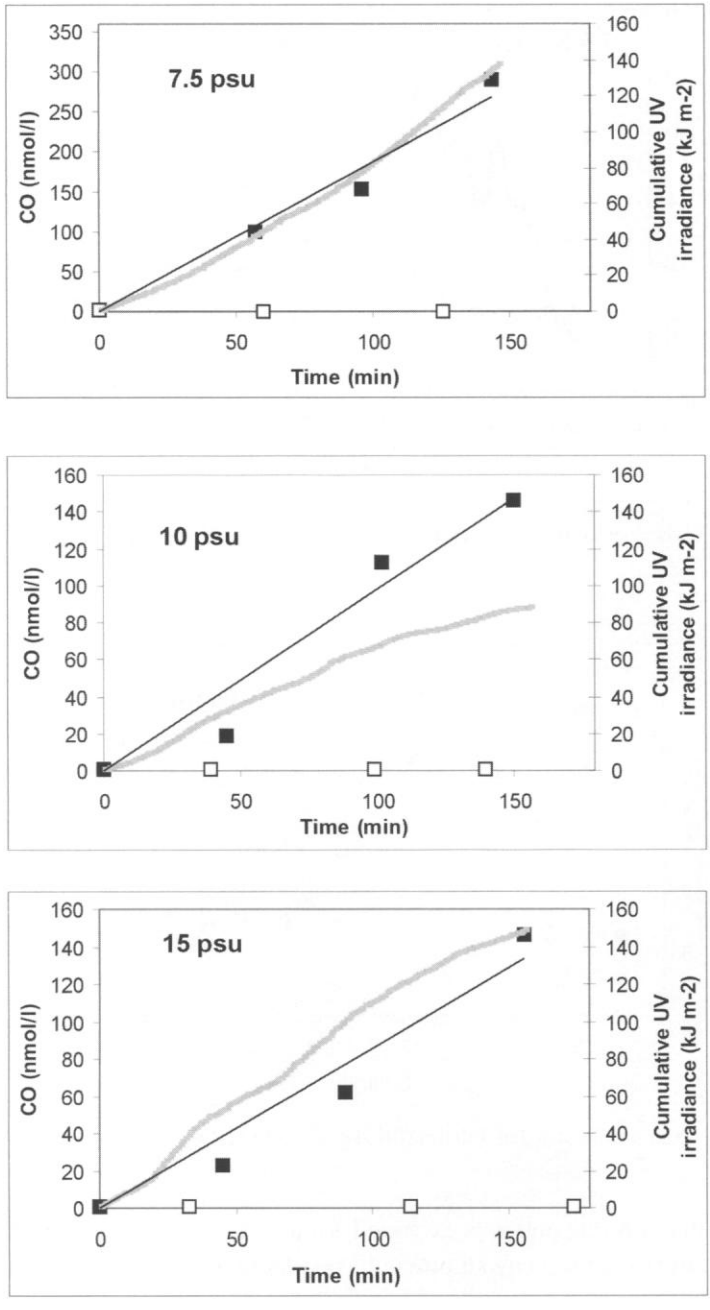


*Figure 7.* Potential CO photoproduction (filled squares) at salinities 7.5, 10 and 15 in May. Note the different CO concentration scale at the 7.5 salinity station. Controls (open squares) and cumulative irradiance (grey line) are also shown.

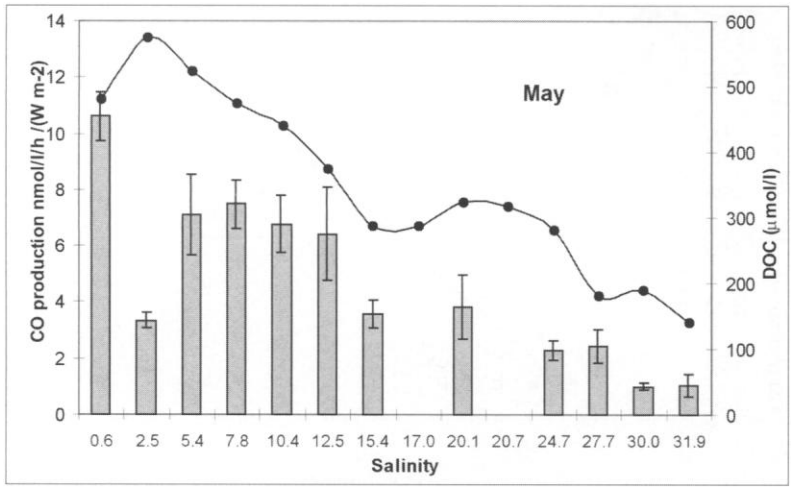


*Figure 8.* Axial profile of mean photoproduction rate (bars) and DOC (filled circles) during May. The uncertainty on the photodegradation rate is the standard error.

measurements on two days during the May survey. Potential photoproduction decreased from 851 nmol $l^{-1}$ $d^{-1}$ in the upper estuary to 92 nmol $l^{-1}$ $d^{-1}$ near the mouth. Rates were normalised to 1 kW-h $m^{-2}$ solar irradiance by scaling daily broad-band UV irradiance to total solar irradiance (9007 kJ $m^{-2}$); normalised photoproduction rate co-varied with [DOC], with a CO production: [DOC] molar ratio range of 0.005–0.0018 (see Figure 9). A similar relationship was recorded for U.S. wetland and lake ecosystems (Zuo & Jones 1997), although CO photoproduction potential was higher in the Scheldt samples (Figure 9), potentially reflecting differences in the photoreactivity of DOC.

Areal CO photoproduction rates were estimated by correcting for the attenuation of UV light in surface waters using the following equation:

$$\int Y\ E0\ e^{-Kd.Z} dz$$

where E0 is shortwave irradiance at the surface in May, Y is the photochemical CO yield per cubic metre per day, Z is depth and Kd the attenuation coefficient at 360 nm. Extrapolating to the estuarine surface area (442 $km^2$) suggests a total photochemical CO production rate of 8.5–18 $\times$ $10^3$ mol $d^{-1}$ for the Scheldt estuary. This is equivalent to 0.21–0.44% of daily terrestrial DOC input during May, when riverine discharge is 100 $m^3$ $s^{-1}$ and riverine [DOC] is 480 $\mu$mol $l^{-1}$. Photolytic DOC loss would be greater with consideration of other photoproducts. Dissolved inorganic carbon (DIC) is produced

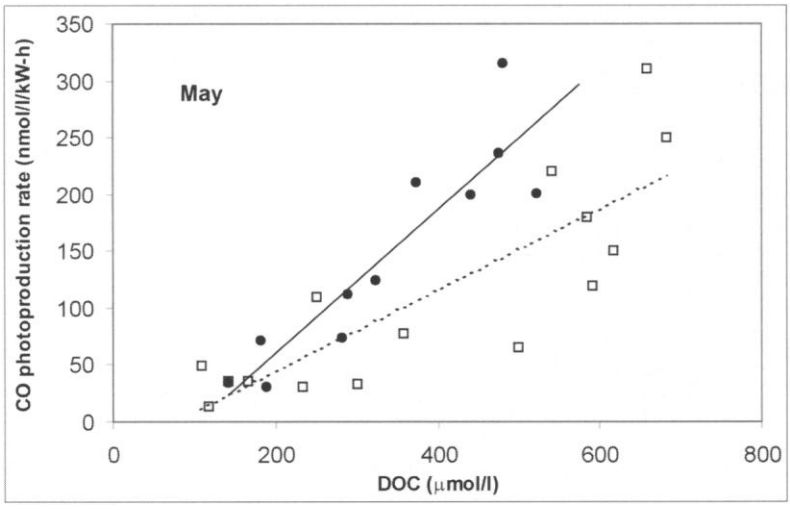


*Figure 9.* Relationship between CO photoproduction rate (normalised to 1 kW-h) and DOC for the Scheldt estuary during May (filled circles) and U.S. lake and wetland sites (open squares) (Zuo & Jones 1997).

by photochemical decarboxylation of DOC at a DIC:CO ratio of 15:1 (Miller & Zepp 1995), and LMW carbonyl compounds such as formaldehyde, acetaldehyde and glyoxylate are formed at an approximately equal rate to CO (Mopper et al. 1991; Moran & Zepp 1997). Using CO production as a proxy and assuming that the photoproduct ratio remains constant suggests a total photolytic loss equivalent to 5.5% of the daily DOC input to the Scheldt. DOC photodegradation could account for an equivalent of 0.005–0.021% of the total column-integrated DOC in the Scheldt, consistent with estimates of 0.01% for the Amazon River (Amon & Benner 1996).

## Discussion

### *Air-Sea exchange of CO*

The axial [CO] profiles demonstrate that the outer estuary is the primary site for atmospheric emission. This was particularly striking in spring and summer, when outer estuary emissions were four-fold and an order of magnitude greater than upper estuary fluxes (Figure 10). A similar trend was apparent in October, although mean fluxes were an order of magnitude lower. Whereas higher windspeeds will enhance exchange during winter, the estuary was only a minor source of CO in December while the mid-estuary was a

minor sink. The elevated CO emission from the headwaters in autumn and winter (Figure 10) may reflect equilibration of river water with continental air masses of higher CO upstream of the estuary. It should be noted that the uncertainty on the emissions is relatively high, as it accounts for both the uncertainty in k (40%, Clark et al. 1995), and variability in the mean atmospheric CO (see Table 1).

The Scheldt CO emissions of 4–404 nmol $m^{-2}$ $h^{-1}$ (Table 2) are relatively low in comparison with the oceanic range of 250–1300 nmol $m^{-2}$ $h^{-1}$ (Bates et al. 1995). There are few estimates of coastal CO fluxes for comparison, although the Scheldt emissions were lower than the mean of 843 nmol $m^{-2}$ $h^{-1}$ (range 380–1520 nmol $m^{-2}$ $h^{-1}$) obtained in Yaquina Bay, Oregon (Butler et al. 1987). Comparison with total DOC loading suggests that CO emissions only account for 0.033% (0.02–0.05%) of DOC input (Table 2). Despite the industrialised catchment and pronounced upstream oxygen sag, the Scheldt DOC and SPM range are typical of European and American estuaries (see Abril et al. in press, Table 8; Miller 1999, Table 3). This supports the use of the Scheldt CO emissions to obtain an estimate of regional and global estuarine emissions in the absence of CO emission data from other estuaries. Extrapolation of the mean spatially-integrated CO flux (see Table 2) to the European and global estuarine surface area ($0.11 \times 10^6$ and $1.4 \times 10^6$ $km^2$, respectively; Woodwell et al. 1973; Woodwell 1980) provides respective estuarine emissions of 5 (2.7–7) and 64 (35–90) Gg CO $y^{-1}$. These estimates should be regarded as lower limits, as the Scheldt receives less incident UV radiation than larger low-latitude estuaries such as the Amazon and Orinoco, and the Scheldt SPM loading is high compared with other estuaries (Uncles et al. in prep.). The estimated global estuarine emission suggests that an equivalent of 0.48% (0.27–0.7%) of the oceanic CO flux (12.9 Tg $yr^{-1}$; Bates et al. 1995) originates from estuaries, which occupy 0.38% of the surface area of the global ocean. Although the uncertainty in extrapolating to the global estuarine surface area is large, the results indicate that the estuarine contribution to global CO emissions is not significant.

*Microbial CO oxidation and cycling*

The distribution of CO in the surface ocean is primarily controlled by microbial oxidation (Johnson & Bates 1996), with CO consumption dominating in the euphotic zone in the absence of light (Jones et al. 1984). As microbial oxidation was not detected in the photoproduction controls (see Figure 7), oxidation rates were estimated indirectly for each 2.5 salinity sector by subtracting the CO emission rate from the photoproduction rate (Figure 11). This was based on the assumption that emission and oxidation rates remained constant over a 24-hr day, with the CO produced during

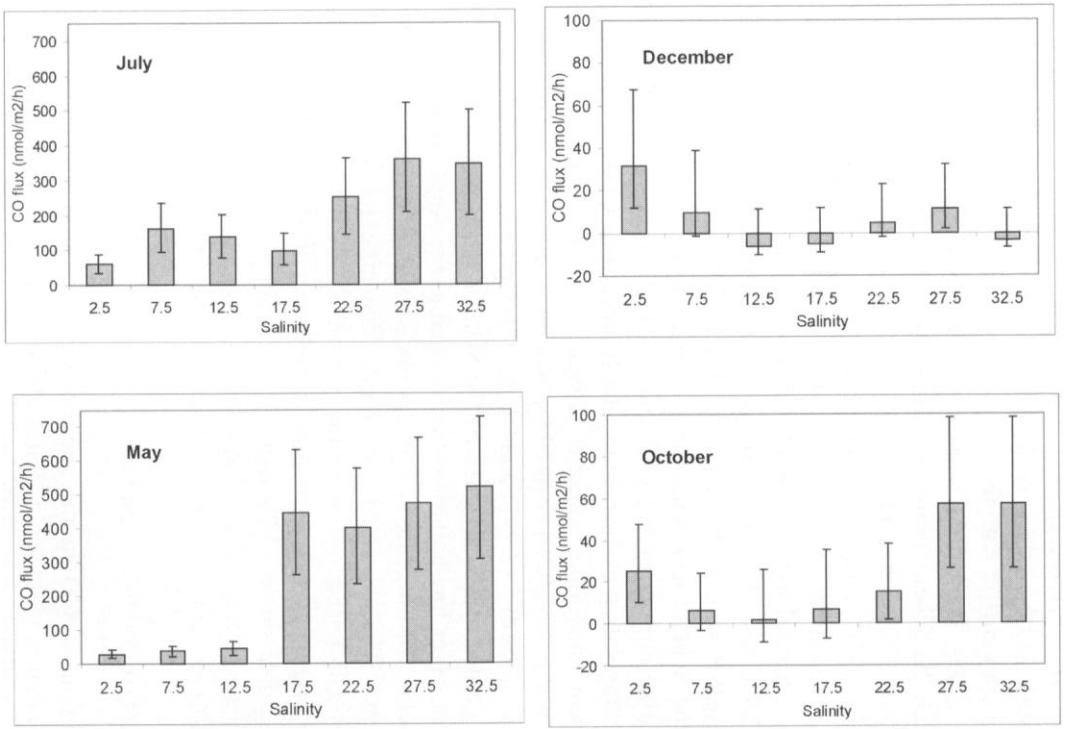


*Figure 10.* Axial profiles of seasonal CO atmospheric emissions in each salinity sector. Note the y-axis scale change between spring-summer and autumn-winter. The error bars represent the combined error in the estimate of k (40%; Clark et al. 1995), and the uncertainty in the mean atmospheric CO from which $CO_E$ was calculated (see Table 1).

*Table 2.* Seasonal and annual total CO emissions and predicted % DOC loss. Fluxes were estimated on a basis of 91.25 days/season, and DOC loading on the measured upper estuary end-member [DOC] for each survey

| Survey | Month | Mean spatially-corrected CO flux nmol $m^{-2}$ $h^{-1}$ | Total CO emission $10^3$ mol | Flow $m^3$ $s^{-1}$ (Baeyans et al. 1998) | DOC load $10^9$ mol C | CO flux as a % of total C loading |
|---|---|---|---|---|---|---|
| Scheldt1 | July | 275.8 (159–401) | 267.2 (154–388) | 60 | 0.22 | 0.12 (0.07–0.17) |
| Scheldt2 | December | 3.8 (–3–23) | 3.7 (–2.9–22) | 180 | 0.85 | 0.0004 (–0.0003–0.003) |
| Scheldt3 | May | 403.8 (237–569) | 391.1 (230–551) | 100 | 0.38 | 0.1 (0.06–0.15) |
| Scheldt4 | October | 38.8 (15–73) | 37.6 (14.5–71) | 120 | 0.65 | 0.006 (0.002–0.011) |
| Annual | Total | 180.5 (102–266) | 699.7 (396–1032) | – | 2.10 | 0.033 (0.02–0.05) |

DOC photodegradation mixed throughout the water column. Oxidation was assumed to be uniform throughout the water column, and riverine CO input in the upper estuary and export to shelf waters were not considered. CO oxidation primarily accounted for CO photoproduction in the upper estuary (see Figure 11(a)), with maximum oxidation rates of 0.25 nmol $l^{-1}$ $h^{-1}$ declining to 0.01 nmol $l^{-1}$ $h^{-1}$ in the outer estuary. This is relatively low in comparison to the rates of 1.14 and 0.14 nmol $l^{-1}$ $h^{-1}$ at salinities 2.2 and 33 in Yaquina Bay (Jones et al. 1984), and 0.61–0.97 nmol $l^{-1}$ $h^{-1}$ off the Orinoco mouth (Jones & Amador 1993). However the observation that CO production and consumption are of similar order in the upper estuary is consistent with the rapid CO turnover observed at low salinities in Yaquina Bay (Butler et al. 1987). When considered on an areal basis (see Figure 11(b)), the results suggest that atmospheric emission and microbial oxidation account for 32% and 68%, respectively, of the CO produced by photodegradation of DOC in the Scheldt estuary. For comparison, microbial oxidation is reported to account for 10–20% of CO photoproduction in the surface ocean (Mopper et al. 1991; Zuo & Jones 1998).

CO oxidation in the ocean is attributed to ammonium and methane oxidisers, which utilise CO as an alternative substrate for the ammonium monoxygenase system (Jones et al. 1984). Previous studies of estuarine CO

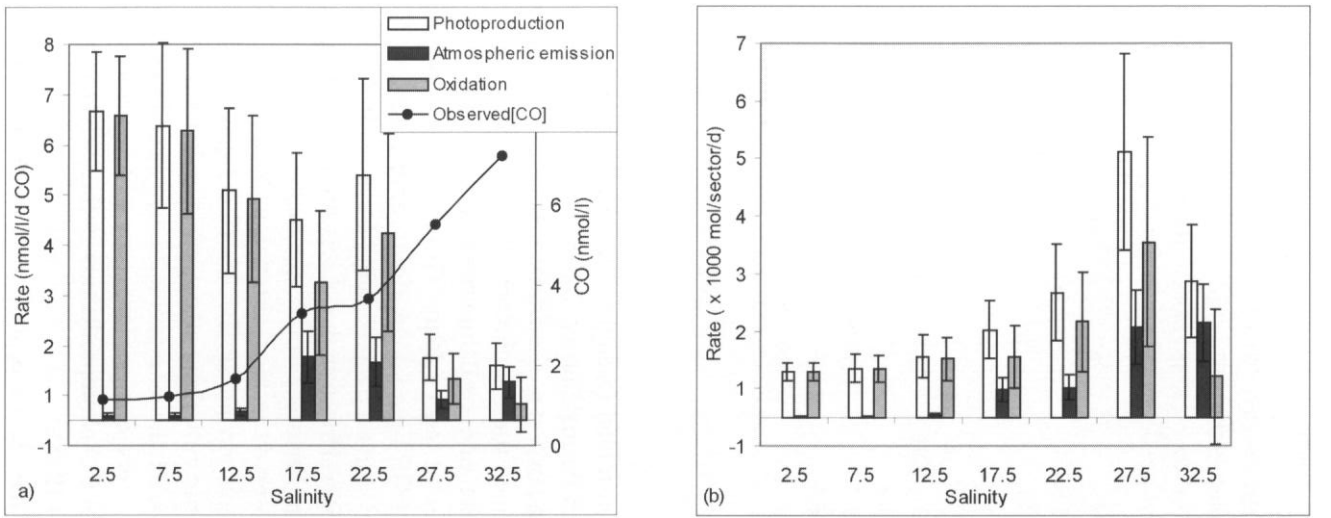


*Figure 11.* CO fluxes for each 2.5 salinity sector of the Scheldt estuary expressed as (a) CO increase per unit volume due to photoproduction (white), and CO decrease per unit volume due to atmospheric emission (black) and oxidation (grey) and (b) total areal photoproduction (white), emission (black) and oxidation (grey). Mean [CO] is shown in (a) for comparison. The uncertainty on the photoproduction is the standard deviation about the mean of all photoproduction rate estimates within each sector. The uncertainty on the emission estimates is the combined error in the estimate of k (40%; Clark et al. 1995), and the uncertainty in the mean atmospheric CO from which $CO_E$ was calculated (see Table 1). The error on the oxidation is the summed error on the photoproduction rate and emission rates.

oxidation suggest that 69–88% is attributable to nitrification (Jones et al. 1984), which is maximal at salinities of 1–2 in the Scheldt estuary (De Wilde & De Bie 2000). As ammonium oxidiser biomass co-varies with SPM concentration in estuaries (Owens 1986), the SPM distribution may also reflect CO oxidation potential. Consequently the observed coincidence of SPM maxima and [CO] minima in May and July may be due to the combined effect of reduced light penetration and an enhanced microbial CO sink associated with particles. This may explain why CO oxidation was insignificant in the photo-irradiation control samples (see Figure 7), as particles were partially excluded in the controls. If SPM does influence [CO], this suggests that decreased suspended loading, due to improved water treatment or change in industrial/agricultural activities for example (Wollast 1988), could result in an increase in estuarine CO production and emissions. Alternatively CO loss may have been insignificant in the controls as the main site for oxidation in the upper estuary is the surface sediment, as observed for nitrification (N. Iversen, pers. comm.).

*Photoproduction of CO*

Light is absorbed in surface waters primarily by chromophoric dissolved organic matter (CDOM), which is defined as a 'chemically complex and ill-defined mixture of anionic organic oligoelectrolytes that contain phenolic compounds' (Aiken et al. 1985). Humic substances constitute the bulk of the CDOM, and are derived from terrestrial plant lignin, a phenolic compound which degrades to aromatics and ketones, and represents the major source of photochemical precursors for low molecular weight (LMW) carbonyl compounds and CO (Kieber et al. 1990; Zuo & Jones 1997). CO production has been correlated with humic concentration (Mopper et al. 1991), and production of LMW compounds and CO are enhanced by addition of carbonyl and phenolic compounds (Kieber at al. 1990; Zuo & Jones 1997). As freshwater DOM exhibits a higher CO photoproduction efficiency than marine DOM (Zuo & Jones 1997) it is not surprising that photoproduction potential was highest in the upper estuary and declined at higher salinities (Figure 8). This is not simply a function of dilution however, as CDOM absorbance and photoreactive capacity are also reduced as salinity increases due to other physico-chemical reactions. Flocculation in the Scheldt estuary occurs between salinities of 1 and 5 (Wollast 1988), and it is estimated that this process removes ~65–80% of dissolved riverine humic acids in major estuaries (Sholkovitz et al. 1978). Although this only accounts for 3–6% of total DOC, it represents a major fraction of the CDOM, and so a relatively more photo-labile DOC pool would be present in the upper estuary as confirmed by the photoproduction potential experiments. Higher concentra-

tions of dissolved iron also enhance photochemical production of CO *via* the formation of stable organic complexes with elevated photoreactivities (Zou & Jones 1997). Consequently the removal of dissolved iron at salinities <15 (Sholkovitz et al. 1978) could also account for the observed decrease in CO photoproduction capacity in the lower estuary (see Figure 8). The photoproductivity of freshwater humics may be enhanced in the presence of transient reactive species from seawater, as reported for carbonyl sulphide production (Zepp & Andreae 1994), although the trend in photoproduction potential in the Scheldt suggests that this is not critical to CO production.

A correlation between normalised CDOM absorbance and photoproduction rates for dissolved and volatile species has been reported for a range of biogeographic ecosystems (Kieber et al. 1990; Valentine & Zepp 1993). This has led to suggestions that CDOM absorbance can be used as a predictive proxy for photo-production and emission of CO and carbonyl sulphide (Valentine & Zepp 1993; Uher & Andreae 1997). Although CDOM absorbance was not measured in this study it can be assumed that it is higher in the upper estuary and declines with increasing salinity, in which case estimates of estuarine CO emissions based upon a linear relationship with CDOM absorbance would not reflect actual emissions. Although the potential exists for the prediction of photoreactivity from the retrieval of CDOM spectra by remote-sensing, caution is required in the application of absorption:photoproductivity relationships to the distribution and air-sea exchange of CO in estuaries and coastal waters.

Light attenuation would impose a steep gradient in CO photoproduction in the surface water of the estuary. However, vertical stratification in the Scheldt is low (Wollast 1988), and vertical turbulence originating from boundary shear, wind-mixing and tidal effects would distribute the CO throughout the water column. This is confirmed by the high-resolution surface profiles (Figure 4) which provided little evidence of a surface gradient, except in the outer estuary. However preferential enrichment of phenolic material and CDOM may occur in the surface microlayer of estuaries, as a result of elevated natural and anthropogenic surfactant input and CDOM hydrophobicity. This results in a doubling of UV absorbance in surface waters over that of the bulk CDOM in coastal regions (Carlson & Mayer 1980). As greater than 90% of CO photoproduction may occur in the upper 3 cm in wetlands (Valentine & Zepp 1993), the use of 10 cm sampling depths may still have led to an underestimate of CO emissions.

As CO emissions are highest in the outer estuary, estuarine plumes in shelf regions represent further sites for CO production from photodegradation of terrestrial DOC, as reported for LMW compounds (Amon & Benner 1996). Light attenuation will decrease in plume waters, whereas DOC/CDOM will

be elevated relative to the surrounding water. Photoproductive capacity will also be enhanced by the buoyancy of the plume water, with stratification increasing the exposure of CDOM to light. Elevated [CO] in the south-eastern Caribbean is associated with the Orinoco river plume (Jones & Amador 1993), and an inverse correlation has been observed between surface [CO] and salinity in the southern North Sea (Sjoberg 1999). The estimate for the Scheldt estuary then represents a conservative estimate of CO production and terrestrial DOC loss, as it does not include the potentially significant contribution of the plume.

## Acknowledgements

We thank Michelle Loijens and Lei Chou (Universite Libre de Bruxelles), and Sabine Brasse and Max Nellen (University of Hamburg) for the SPM and DOC analysis, and MUMM (Belgium) for the meteorological data. We also acknowledge the help of Greg Jameson for UV spectrophotometric measurements in October, and the officers and crew of the *R/V Belgica*. This study benefitted significantly from the loan of the Delta UV Sensor and irradiation flasks by Guenther Uher, and equilibrator by Hein de Wilde. We are grateful to John Wood for the design and construction of the electronic mainframe and Michel Frankignoulle for exemplary co-ordination of the BIOGEST programme. Finally we thank Guenther Uher, Gerald Moore, Reg Uncles and an anonymous reviewer for advice and comments on the manuscript. This work was funded by the EC Environment programme BIOGEST (ENV4-CT96-0213), and T. Sjoberg was funded by a NERC LOIS studentship (GST/02/370).

## References

Abril G, Nogueira M, Etcheber H, Cabeçadas G, Lemaire E & Brogueira MJ (2002) Behaviour of organic carbon in nine contrasting European estuaries. Est. Coast Shelf Sci., in press

Aiken GR, MacCarthy P, Malcolm RL & Swift RS (1985) Humic substances in soil, sediment, and water: geochemistry and isolation. Wiley, New York

Amon RMW & Benner R (1996) Photochemical and microbial consumption of dissolved organic carbon and dissolved oxygen in the Amazon River system. Geochim. Cosmochim. Acta 60: 1783–1792

Alvarez-Salgado XA & Miller AEJ (1999) Dissolved organic carbon in a large macrotidal estuary (the Humber, NE England): behaviour during estuarine mixing. Mar. Poll. Bull. 37(3–7): 216–224

Baeyans W, van Eck B, Lambert C, Wollast R & Goeyens L (1998) General description of the Scheldt estuary. Hydrobiologia 366: 1–14

Bates TS, Kelly KC, Johnson & Gammon RH (1995) Regional and seasonal variations in the flux of oceanic carbon monoxide to the atmosphere. J. Geophys. Res. 100: 23093–23101

Bekki S, Law KS & Pyle JA (1994) Effect of ozone depletion on atmospheric $CH_4$ and CO concentrations. Nature 371: 595–597

Butler JH, Jones RD, Garber JH & Gordon LI (1987) Seasonal distributions of reduced trace gases in Yaquina Bay, Oregon. Geochim. Cosmochim. Acta 51: 181–203

Cardenas LM, Austin JF, Burgess RA, Clemitshaw KC, Dorling S, Penkett SA & Harrison RM (1998) Correlations between CO, $NO_y$, $O_3$ and non-methane hydrocarbons and their relationships with meteorology during winter 1993 on the north Norfolk coast, U.K. Atmos. Environ. 32: 3339–3351

Carlson DJ & Mayer IM (1980) Enrichment of dissolved phenolic material in the surface microlayer of coastal waters. Nature 286: 482–483

Cicerone RJ (1988) How has the atmospheric concentration of CO changed? In: Rowland FS & Isaksen ISA (Eds) The Changing Atmosphere Dahlem Workshop Reports. J. Wiley and Sons, Chichester

Clark JF, Schlosser P, Simpson HJ, Stute M, Wanninkhof R & Ho DT (1995) Relationship between gas transfer velocities and wind speeds in the tidal Hudson river determined by the dual tracer technique. In: Jahne B & Monahan EC (Eds) Air-Water Gas Transfer (pp 785–800). AEON Verlag and Studio, Hanau

de Wilde HPJ & de Bie MJM (2000) Nitrous oxide in the Schelde estuary: production by nitrification and emission to the atmosphere. Mar. Chem. 69: 203–216

Erikson DJ III (1989) Ocean to atmosphere carbon monoxide flux: Global inventory and climate implications. Global Biogeochem. Cycles 4: 305–314

Evans WFJ & Puckrin E (1995) An observation of the greenhouse radiation associated with carbon monoxide. Geophys. Res. Lett. 22(8): 925–928

Frankignoulle M, Abril G, Borges A, Bourge A, Canon C, DeLille B, Libert E & Theate J-M (1998) Carbon dioxide emissions from European estuaries. Science 282: 434–436

Goosen NK, van Rijswijk P & Brockmann U (1995) Comparison of heterotrophic bacterial production rates in early spring in the turbid estuaries of the Scheldt and the Elbe. Hydrobiologia. 311: 31–42

Hedges JI, Hatcher PG, Ertel JR & Meyers-Schulte KJ (1992) A comparison of dissolved humic substances from seawater with Amazon River counterparts by C-13 NMR Spectrometry. Geochim. Cosmochim. Acta. 56: 1753–1757

Johnson JE & Bates TS (1996) Sources and sinks of carbon monoxide in the mixed layer of the tropical South Pacific Ocean. Global Biogeochem. Cycles. 10: 347–359

Jones RD & Amador JA (1993) Methane and carbon monoxide production, oxidation, and turnover times in the Caribbean Sea as influenced by the Orinoco River. J. Geophys. Res. 98: 2353–2359

Jones RD, Morita RY & Griffiths RP (1984) Method for estimating *in situ* chemolithotrophic ammonium oxidation using carbon monoxide oxidation. Mar. Ecol. Prog. Ser. 17: 259–269

Kieber RJ, Zhou X & Mopper K (1990) Formation of carbonyl compounds from UV-induced photodegradation of humic substances in natural waters: fate of riverine carbon in the sea. Limnol. Oceanogr. 35: 1503–1515

Kromkamp J, Peene J, van Rijswijk P, Sandee A & Goosen N (1995) Nutrients, light and primary production by phytoplankton and microphytobenthos in the eutrophic turbid Westerschelde estuary (The Netherlands). Hydrobiologica 311: 9–19

Law CS, Rees AP & Owens NJP (1992) Nitrous oxide: estuarine sources and atmospheric flux. Est. Coast Shelf Sci. 35: 301–313

Mantoura RFC & Woodward EMS (1983) Conservative behaviour of riverine dissolved organic carbon in the Severn estuary; chemical and geochemical implications. Geochim. Cosmochim. Acta. 47: 1293–1309

Miller AEJ (1999) Seasonal investigations of dissolved organic carbon dynamics in the Tamar Estuary, U.K. Est. Coast Shelf Sci. 49: 891–908

Miller WL & Zepp RG (1995) Photochemical production of dissolved inorganic carbon from terrestrial organic matter – significance to the oceanic organic carbon cycle. Geophys. Res. Lett. 22: 417–420

Mopper K, Zhou X, Kieber RJ, Kieber DJ, Sikorski RJ & Jones RD (1991) Photochemical degradation of dissolved organic carbon and its impact on the oceanic carbon cycle. Nature 353: 60–62

Moran MA & Zepp RG (1997) Role of photoreactions in the formation of biologically labile compounds from dissolved organic matter. Limnol. Oceanogr. 42: 1307–1316

Naijar RG, Erickson III DL & Madronich S (1995) Modelling the air-sea fluxes of gases formed from the decomposition of dissolved organic matter: carbonyl sulfide and carbon monoxide. In: Zepp RG & Sonntag C (Eds) The Role of Non-living Organic Matter in the Earth's carbon cycle. J. Wiley & Sons

Owens NJP (1986) Estuarine nitrification: a naturally occurring fluidized bed reaction? Est. Coast Shelf Sci. 22: 31–44

Scranton MI & McShane K (1991) Methane fluxes in the southern North Sea: the role of European estuaries. Cont. Shelf Res. 11: 37–52

Setser PJ, Bullister JL, Frank EC, Guinasso NL Jr & Schink DR (1982) Relationships between reduced gases, nutrients, and fluorescence in surface waters off Baja California. Deep-Sea Res. I 29: 1203–1215

Sholkovitz ER, Boyle EA & Price NB (1978) The removal of dissolved humic acids and iron during estuarine mixing. Earth Plan. Sci. Lett. 40: 130–136

Sjoberg TN (1999) The distribution and cycling of dissolved carbon monoxide in estuarine, coastal and shelf break environments. Ph.D. thesis. The University of East Anglia, 250 pp

Sze NK (1977) Anthropogenic CO emissions: implications for the atmospheric CO-OH-$CH_4$ cycle. Science 195: 673–675

Uher G & Andreae MO (1997) Photochemical production of carbonyl sulfide in North Sea water: A process study. Limnol. Oceanogr. 42: 432–442

Uncles RJ, Stephens JA & Smith RE (submitted) The dependence of estuarine turbidity on tidal intrusion length, tidal range and residence time. Cont. Shelf Res.

Valentine RL & Zepp RG (1993) Formation of carbon monoxide from the photodegradation of terrestrial dissolved organic carbon in natural waters. Environ. Sci. Technol. 27: 409–412

Watson RT, Rodhe H, Oeschger H & Siegenthaler U (1990) Greenhouse gases and Aerosols. In: Houghton JT, Jenkins GJ & Ephraums JJ (Eds) Climate Change: The IPCC Scientific Assessment Eds. Cambridge University Press

Weisenburg DA & Guinasso NL (1979) Equilibrium solubilities of methane, carbon monoxide and hydrogen in water and seawater. J. Chem. and Eng. Data 24: 354–360

Williams PM & Druffel ERM (1987) Radiocarbon in dissolved organic matter in the central North Pacific Ocean. Nature 330: 246–248

Wise DL & Houghton G (1968) Diffusion coefficients of neon, krypton, xenon, carbon monoxide and nitric oxide in water at 10–60 °C. Chem. Eng. Sci. 23: 1211–1216

Wollast R (1988) The Scheldt estuary. In: Salomans W, Bayne BL, Duursma EK & Forstener U (Eds) Pollution of the North Sea: an assessment. Springer-Verlag, pp 185–193

Woodwell GM (1980) Aquatic Systems as part of the biosphere. In: Barnes RSK & Mann HH Fundamentals of Aquatic Ecosystems. Blackwell Sci. Publ., pp 201–215

Woodwell PM, Rich PH & Hall CAS (1973) In: Woodwell PM & Pecan EV (Eds) Carbon and the Biosphere. U.S. National Technical Information Service, Springfield, VA, pp 221–240

Zepp RG & Andreae MO (1994) Factors affecting the photochemical production of carbonyl sulfide in seawater. Geophys. Res. Lett 25: 2813–2816

Zou Y & Jones RD (1997) Photochemistry of natural dissolved organic matter in lake and wetland waters – production of carbon monoxide. Wat. Res. 31: 850–858

Zou Y & Jones RD (1998) Reassessment of the ocean-to atmosphere flux of carbon monoxide. Chem. Ecol. 14: 241–257